Supporting Information

Self-assembly of Water-filled Molecular Saddles to Generate Diverse Morphologies and High Proton Conductivity

Nyaya Prakash Pradhan,[a] Sweety Gupta,[†a] Swapnendu Narayan Ghosh,[†b] Amit Paul*,[a] Santanu Talukder*,[b] Aasheesh Srivastava*[a]

[a] *Department of Chemistry, Indian Institute of Science Education and Research Bhopal (IISER Bhopal), Bhauri, Bhopal Bypass Road, Bhopal, 462 066, Madhya Pradesh, India.*

[b] *Department of Electrical Engineering and Computer Science, Indian Institute of Science Education and Research Bhopal (IISER Bhopal), Bhauri, Bhopal Bypass Road, Bhopal, 462 066, Madhya Pradesh, India.*

Table of Content:

1. Materials and Methods

1.1 *General Information*

All the chemicals and solvents used for synthesis and characterization were purchased from commercial suppliers such as Sigma-Aldrich, Spectrochem, TCI Chemicals, BLD Pharm, and Merck. No additional purification was performed before using them. Autoclaved Mili-Q water was used to prepare the SEM and TEM samples.

1.2 *Methods and Instrumentations*

High-Resolution Mass Spectrometry (HRMS)− The HR-MS data of the compounds were recorded using Bruker MicroTOF-Q-II mass spectrophotometer using electrospray ionization (ESI) mode. The samples were prepared by dissolving 1 mg of the respective compound in organic solvents like DCM, MeOH, and $CHCl_3$. Then, 2 µL of the sample was inserted into the column directly and run for 6 minutes.

Nuclear Magnetic Resonance (NMR)− ^{1}H and ^{13}C Nuclear Magnetic Resonance (NMR) studies were performed on Bruker Ultra Shield (500 MHz) spectrometer. For NMR sample preparation, 10-12 mg of the compound was dissolved in 0.5 mL of deuterated solvents like DMSO-d_6 and $CDCl_3$.

Single Crystal X-Ray Diffraction (SC-XRD)− Single Crystal X-ray Diffraction data were recorded on a Bruker D8 Venture diffractometer equipped with a Photon-III detector using S4 monochromated Mo Kα radiation (λ = 0.71073 Å) at 140 K using an Oxford cryo-stream low-temperature device. Bruker APEX II software was used for unit cell measurement, data integration, scaling, and absorption corrections for the crystal. Data reduction was done using the SAINT suite from Bruker. Absorption correction was carried out using the multi-scan method implemented in SADABS. All the crystal structures were solved by direct methods using SIR 2014. The crystal structure refinements were done in the program package OLEX2.[1]

DFT Calculations− The energy optimization of the compound was performed through DFT calculations at the B3LYP level combined with 6-311G++(d,p) basis sets using Gaussian 09 program.[2] The frontier molecular orbital representations were generated using the GaussView 6.0 molecular visualization program.

Field Emission Scanning Electron Microscopy (FESEM)− The morphology of the sample under different conditions was characterized using Carl Zeiss (Ultra plus) field emission scanning electron microscope (FESEM). Samples for microscopy were prepared by drop-casting 20 µL of the respective sample on a cover glass slip. The stubs were dried inside a vacuum desiccator at RT for 12 h and then coated with gold for 120 s.

Transmission Electron Microscopy (TEM)− The morphology of samples was further investigated using the FEI TALOS 200S instrument, operating at a voltage of 200 kV. The sample for TEM analysis was prepared by drop-casting samples over a carbon-coated 400 mesh Cu grid and stained with freshly prepared 0.3% w/v phosphotungstic acid (PTA) for 120 seconds. The grid was then dried inside a vacuum desiccator at RT for 12 h.

Electron Paramagnetic Resonance (EPR)− The EPR spectra for the sample were acquired using a Bruker BioSpin GmbH spectrometer operating at a microwave frequency of 9.4 GHz within the X band. For the solid-state EPR experiment, 50-60 mg of solid sample was directly taken in an EPR tube, and data was recorded at 140 K.

Conductivity Measurements− The BioLogic SP240 instrument was used to perform Electrical Impedance Spectroscopy (EIS) techniques to obtain proton conductivity data of the pelletized sample. The temperature and humidity were controlled throughout the experiment using an ESPEC temperature-humidity programmable chamber (Model SH-222). All experiments for the pellet sample were conducted using a two-probe setup in the frequency range of 5 MHz to 1 Hz. The AC proton conductivity of the crystal sample was measured using a HIOKI IM3536 LCR meter in the frequency range of 1 MHz to 1 kHz, and the DC conductivity was measured using a Keithley 2450 source measurement unit (SMU).

2. Synthesis and Characterization

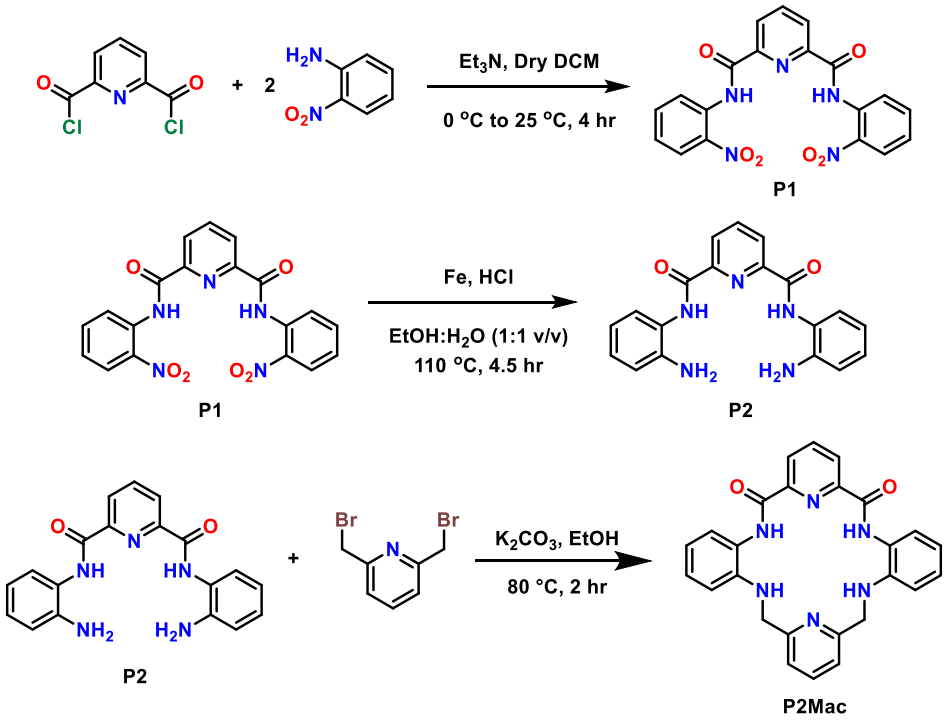

Scheme S1: Synthetic route of the macrocycle **P2Mac**.

The precursor **P2** was synthesized following a previously reported protocol.[3] As shown in scheme S1, initially, precursor **P1** was synthesized by condensing pyridine-2,6-dicarbonyl dichloride with 2-nitroaniline in a 1:2 molar ratio, and then it was reduced using Fe/HCl to obtain precursor **P2** with 70-80% yield.

Synthesis of 3,5,9,11-tetraaza-1,7(2,6)-dipyridina-4,10(1,2)-dibenzenacyclododecaphane-2,12-dione (P2Mac)

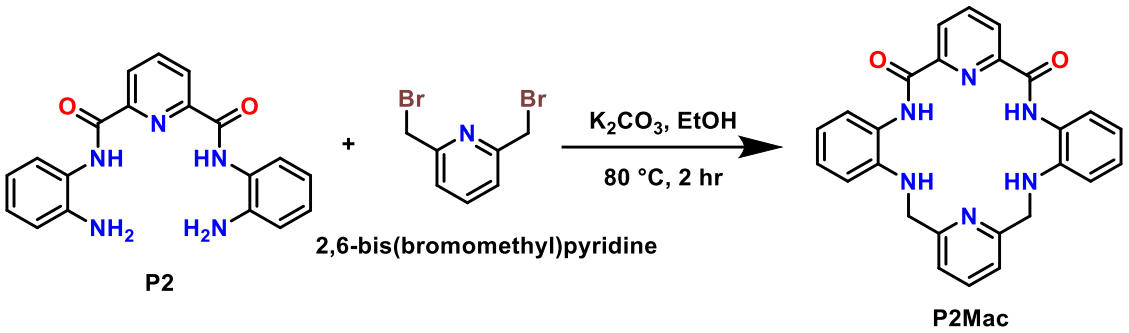

Scheme S2: Synthesis of **P2Mac**.

In a 50 mL round bottom flask, precursor **P2** (400 mg, 1.15 mmol), 2,6-bis(bromomethyl)pyridine (305 mg, 1.15 mmol), and K_2CO_3 (478 mg, 3.46 mmol) were added to 25 mL EtOH and heated at 80 °C. The progress of the reaction was monitored through TLC. After 2 hours, the reaction mixture was cooled, and the solvent was removed under reduced pressure. The solid was then dissolved in $CHCl_3$ and extracted twice with $CHCl_3/H_2O$, and the organic layer was dried over sodium sulphate. The solvent was evaporated under reduced pressure and purified using column chromatography (0.5% MeOH/$CHCl_3$) to get an off-white colored compound with 35% yield. **^{1}H NMR** (500 MHz, DMSO-d_6) δ_{ppm} = 10.92 (s, 1H), 8.34 (d, J = 7.2 Hz, 2H), 8.26 (dd, J = 8.2, 7.2 Hz, 1H), 7.82 (t, J = 7.6 Hz, 1H), 7.43 (t, J = 8.3 Hz, 4H), 7.24 (t, J = 7.8 Hz, 2H), 6.96 (d, J = 8.2 Hz, 2H), 6.83 (t, J = 7.6 Hz, 2H), 5.59 (t, J = 4.8 Hz, 2H), 4.34 (d, J = 4.8 Hz, 4H); **^{13}C NMR** (126 MHz, DMSO-d_6) δ_{ppm} = 162.46, 157.60, 149.16, 143.34, 140.38, 138.41, 128.31, 127.79, 125.46, 123.70, 122.22, 117.53, 112.41, 49.04; **HRMS** (ESI) Calcd. for $C_{26}H_{22}N_6O_2$ $(M+H)^+$: 451.1877, Found: 451.1882.

3. Single Crystal X-Ray Diffraction (SC-XRD) Studies

Single rod-shaped crystals of **P2Mac** were obtained through the vapor diffusion technique. To obtain appropriate crystals for X-ray diffraction, ethyl acetate vapors were gradually infused into the THF solution of **P2Mac** over a period of 2-3 days at 277 K. Crystal data were then solved and refined using the OLEX2 software package. All the crystallographic parameters of the molecule are provided below in Table S1.

3.1 Crystallographic Data

Table S1. Crystal data and structure refinement for **P2Mac**⊃H_2O.

Formula	C_{26} H_{24} N_6 O_3
Formula Weight	468.51
Temperature (K)	296
Crystal System	Monoclinic
Space Group	$P2_1/n$
Z	4
***a* (Å)**	15.1491(13)
***b* (Å)**	8.2400(6)
***c* (Å)**	17.9700(13)
***α* (°)**	90
***β* (°)**	91.932(4)
***γ* (°)**	90
Volume ($Å^3$)	2241.9(3)
Density (g cm^{-3})	1.388
F (000), μ (mm^{-1})	984.0, 0.094
θ (min, max) (°)	2.27, 29.13
$h_{min, max}$, $k_{min, max}$, $l_{min, max}$	(-20,20), (-11,11), (-24,24)
Radiation	Mo Kα (λ = 0.71073 Å)
Reflections collected	6029
Final R indexes (all data)	R_1 = 5.39, wR_2 = 14.45
G.o.F	1.013
CCDC	2326935

3.2 Crystal Structure Analysis of P2Mac⊃H₂O

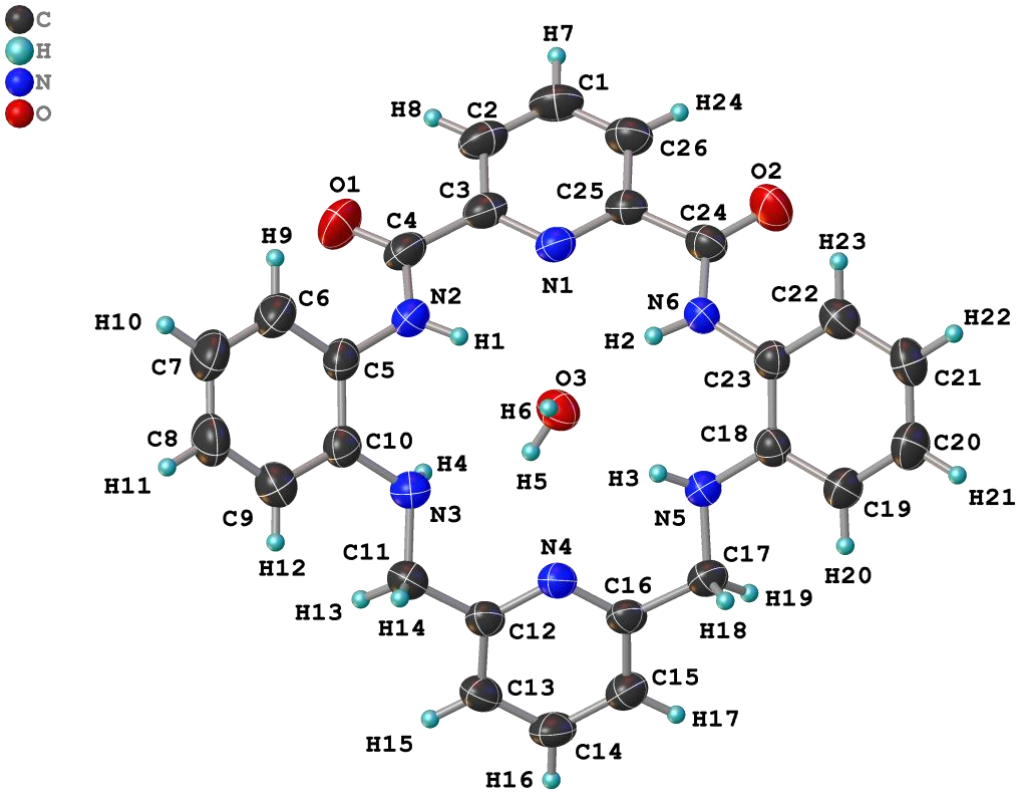

Fig. S1 ORTEP diagram of **P2Mac**⊃H_2O at 50% probability.

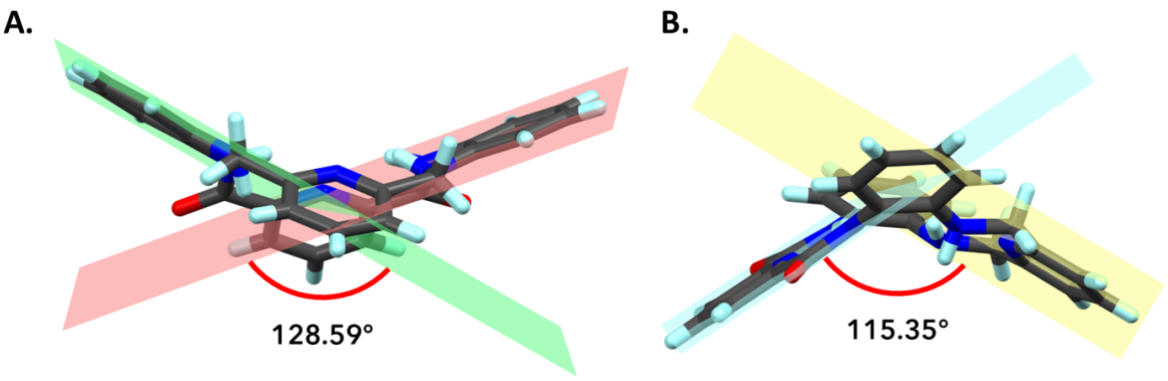

Fig. S2 Crystal structure of **P2Mac** illustrating the dihedral angle between the planes formed by **(A)** phenyl and **(B)** pyridine residues.

H-bond donor & acceptor distances	
H-bonds	**Distances (Å)**
N2-H1···N1	2.727
N6-H2···N1	2.748
N2-H1···O3	3.059
N6-H2···O3	3.002
N5-H3···O3	2.960
O3-H5···N3	2.923
O3-H5···N4	3.064
O3-H6···N5*	2.842

* *Intermolecular H-bond*

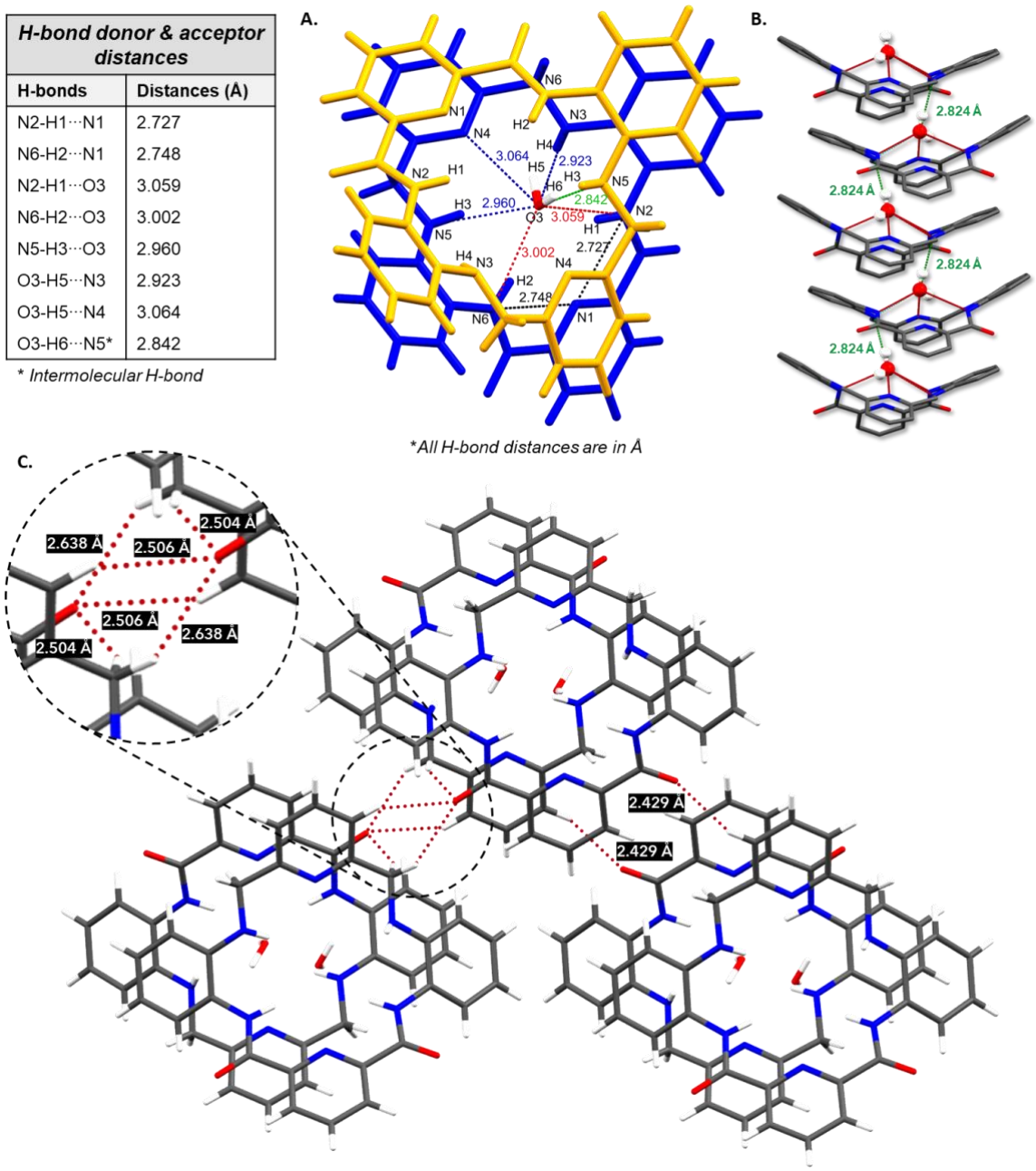

Fig. S3 (A) Illustration of H-bonding network of **P2Mac** crystals with H_2O molecule. **(B)** Molecular packing of **P2Mac** along the *b*-axis showing stacked water channel. **(C)** Top view of crystal packing along the *b*-axis displaying intermolecular short contact interaction.

For preparing rod-shaped crystals of **P2Mac**, 20 µL H_2O was added to 1 mL THF solution of the compound. Subsequently, vapors of ethyl acetate were gradually diffused into the solution over a period of three days at 4 °C.

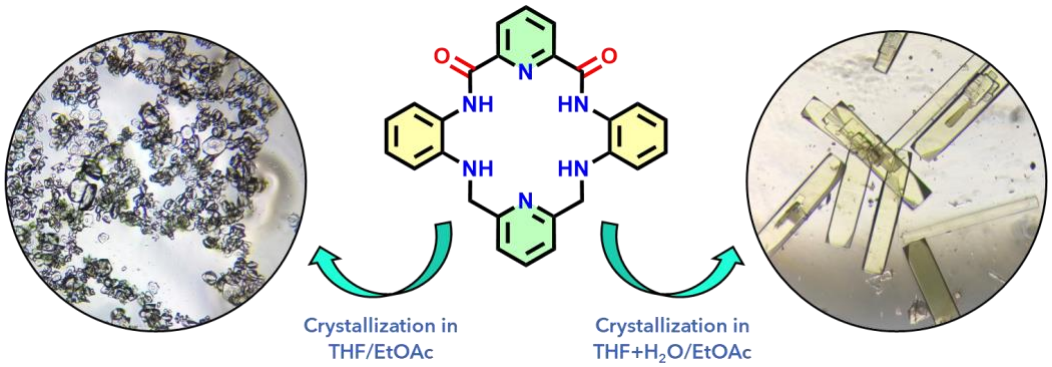

Fig. S4 Representation of the formation of **P2Mac** crystals in various shapes under different crystallization conditions.

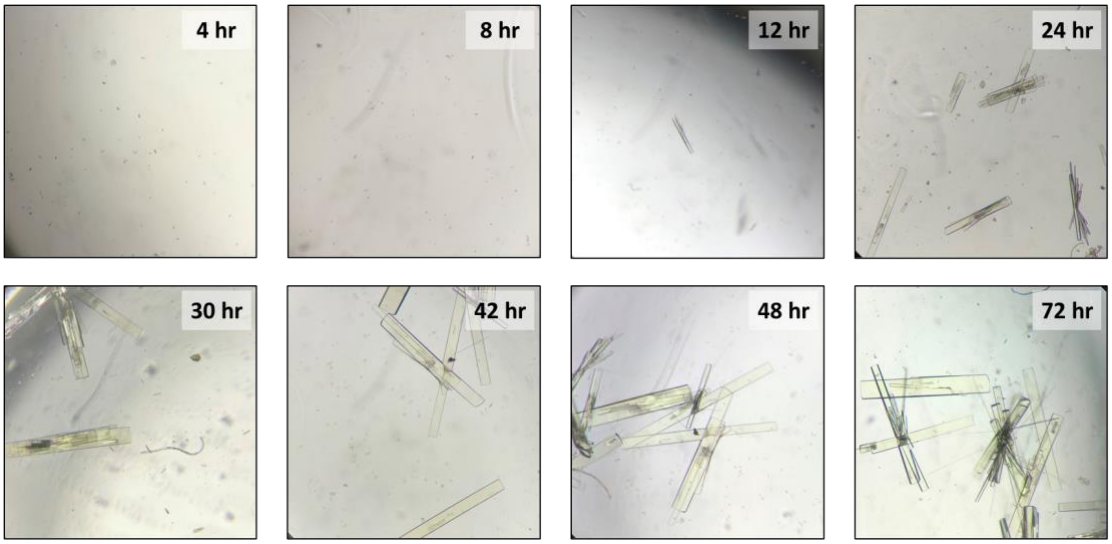

Fig. S5 Microscopic images from a time-dependent crystal growth experiment illustrating the progression of rod-shaped crystal growth in the THF/EtOAc solvent system containing 2% water.

4. EPR Studies

The EPR experiment was conducted in the presence and absence of UV light using a solid sample of **P2Mac** at 140 K. The Lande factor (g) was calculated from the following equation (1):

$$g = \frac{h\nu}{m_b B} \qquad \text{.....eq (1)}$$

where, h = Planck's constant

ν = Operating frequency of the instrument (9.4 GHz)

m_b = Bohr Magneton

B = Field strength (in Tesla)

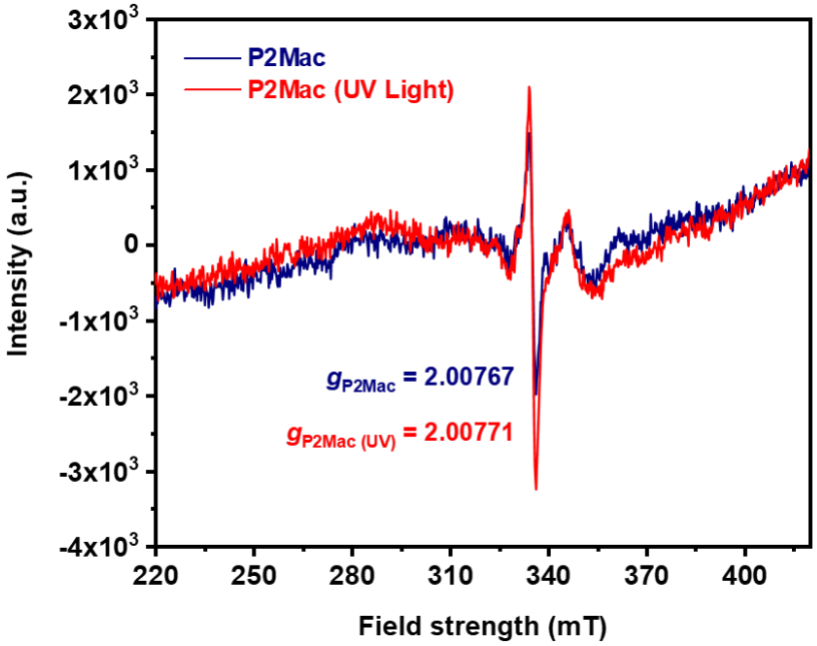

Fig. S6 EPR plot of **P2Mac** in the absence and presence of UV light at 140 K.

5. Morphological Studies

In order to create these diverse morphologies, 900 µL of varying water/THF mixtures were initially taken, and 100 µL THF solution of **P2Mac** (final conc. 0.1 mg/mL) was added at different rates. For creating the hollow nanoparticles, 100 µL THF solution of **P2Mac** was added gently on top of the water/THF mixture for a duration of 60 sec (100 µL/60 sec) and kept steady for 1 hour (final volume ratio of 50% v/v water/THF). After 1 hour, the solution was shaken gently, and 20 µL of the sample was then dropped cast on the SEM stub fitted with a glass coverslip or TEM grid (see Fig. S7 below). The microrods were prepared by instantly adding the THF solution of **P2Mac** (@100 µL/sec) into the water/THF mixture. However, for the octahedron and hexapod preparation, the compound THF solution was added gently (@100 µL/30 sec) to different water/THF mixtures (30% and 90% v/v, final ratio, respectively) and shaken mildly for a few seconds.

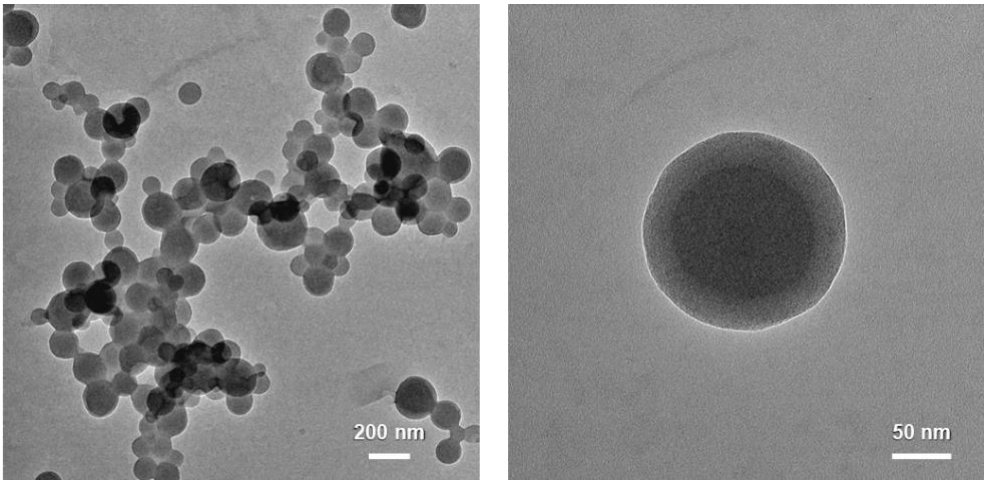

Fig. S7 TEM images of the hollow nanoparticles of **P2Mac** formed at 50% water/THF solution through a slow addition process.

6. Proton Conductivity Studies

6.1 Proton Conductivity Study of Pelletized Sample

Powder samples of **P2Mac** (80 mg) were compressed into pellets of 13 mm diameter using a hydraulic press. The thickness of the pellet was 0.52 mm, measured by a screw gauge. The pellet was kept in an environment of aqueous HCl (ca. 5.5 M) for 4 h and subsequently placed in a two-probe cell, which was then placed inside the temperature humidity programmable chamber. Prior to the experiment, the pellet was equilibrated for 12 hours in a particular humidity condition. For the temperature-dependent experiment, the sample was kept at equilibrium for 1 hour at each temperature.

The AC proton conductivity of **P2Mac** was calculated using the following equation:

$$\sigma = \frac{1}{R2} \times \frac{l}{A} \qquad \text{……eq (2)}$$

where, $R2$ = Resistance for proton conduction

l = Thickness of the pellet (or length of the crystal)

A = Cross-sectional area

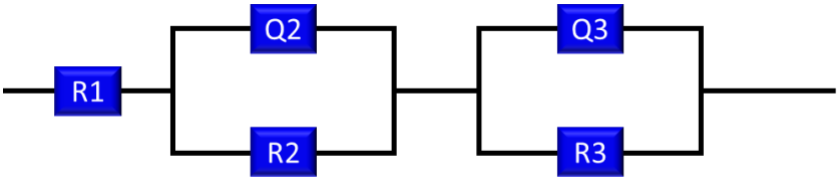

Fig. S8 Circuit used to fit semicircle obtained by EIS measurement to determine the resistance (R2) value.

Fig. S9 (A) Microscopic images of rod-shaped crystals and **(B)** Digital images of the pellets before and after keeping in aqueous HCl environment.

Table S2. Proton conductivity of solid sample at different temperatures at 95% RH.

Sl. No.	*Temperature (°C)*	*Proton conductivity ($mS \cdot cm^{-1}$)*
1	27	2.17×10^{-2}
2	35	3.84×10^{-2}
3	40	6.14×10^{-2}
4	45	7.80×10^{-2}
5	50	1.00×10^{-1}
6	55	1.04×10^{-1}
7	60	1.43×10^{-1}
8	65	1.78×10^{-1}

6.2 Time-dependent Proton Conductivity for Stability Test of P2Mac

The pellet was exposed to 95% RH for a duration of 12 hours, and conductivity measurements were recorded at one-hour intervals over a period of 9 hours. The experiment was repeated three times and the data presented as mean ± standard deviation. The conductivity values are provided in the Table S3.

Table S3. Proton conductivity of pellet sample at different times under 95% RH and 50 °C.

Sl. No.	*Time (hr)*	*Proton conductivity ($\times 10^{-1}$ $mS \cdot cm^{-1}$)*
1	1	1.44 ± 0.15
2	2	1.52 ± 0.05
3	3	1.49 ± 0.04
4	4	1.48 ± 0.12
5	5	1.46 ± 0.09
6	6	1.49 ± 0.08
7	7	1.50 ± 0.11
8	8	1.58 ± 0.04
9	9	1.28 ± 0.15

6.3 ^{1}H NMR Experiment for Stability Test of P2Mac

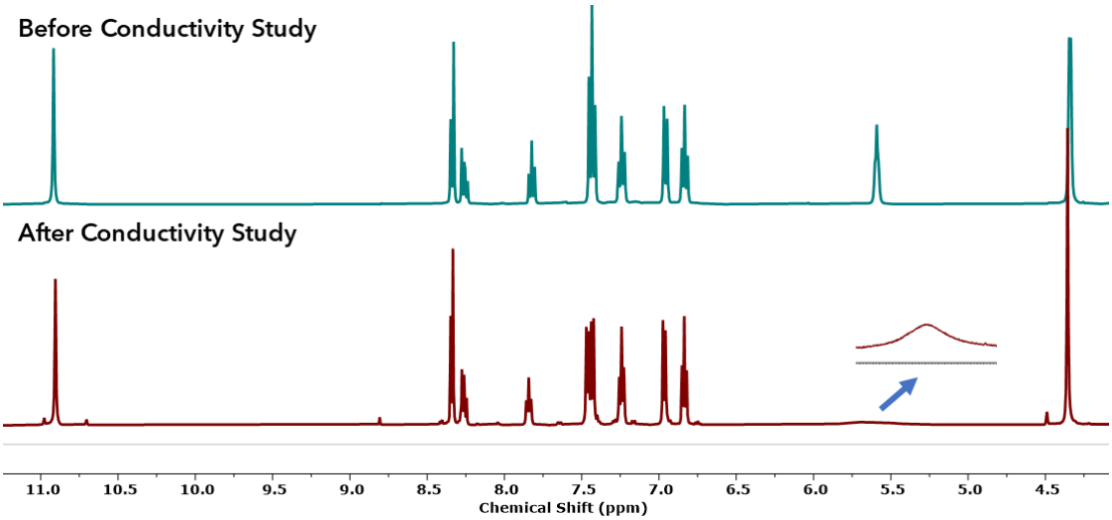

Fig. S10 Stacked ^{1}H NMR plot of **P2Mac** in DMSO-d_6 (500 MHz, 25 °C), before and after proton conductivity study.

6.4 Proton Conductivity Study of Crystal Sample

6.4.1 Preparation of Crystal Sample for Conductivity Studies

As shown in Fig 6D, a thin layer of conductive silver paste was coated on a glass slide. Needles were used to scratch the conductive layer to form grids-like patterns. This helped us to create the contact pads necessary for electrical connections. The crystals of **P2Mac** were then placed on the top of the grids. Once the proper placement of the crystals was confirmed, the samples were kept on a hot plate at ~140 ºC for approximately 30 minutes to allow the silver paste to cure and dry properly. Then, HCl vapors were allowed to diffuse into the crystal for 4 hours before the conductivity measurements.

6.4.2 AC Proton Conductivity Studies

At first, we investigated the AC proton conductivity of the crystal sample by applying an alternating signal of 5 V r.m.s. using an LCR meter. The samples were kept inside an environment-controlled electrical probe station, and the humidity inside the chamber was allowed to rise to ~95% RH over a span of 12 hours. The experimental chamber is vacuum compatible, which ensures an effective isolation and control of the experimental conditions from the room conditions. The electrical connections were made with the help of a pair of sharp tungsten probes attached to a pair of three-axis micromanipulators respectively. The probes were placed on the silver pads to complete the electrical circuit. The frequency of the applied

signal was swept from 1 MHz to 1 kHz, and the corresponding impedance values were noted. Prior to the measurements, the LCR meter was calibrated to remove the cable impedance from affecting the recorded impedance spectrum. The bulk resistance of the crystal was computed to be 63 kΩ and was determined from the Nyquist plot by fitting according to the equivalent circuit shown in Fig. S8. The crystal cross-section area was calculated from the dimensions obtained through SEM imaging, while the distance between the two electrodes was measured from optical micrographs (Fig. S11 and 6D). The AC proton conductivity of the **P2Mac** crystal was calculated using Equation 2, as mentioned earlier.

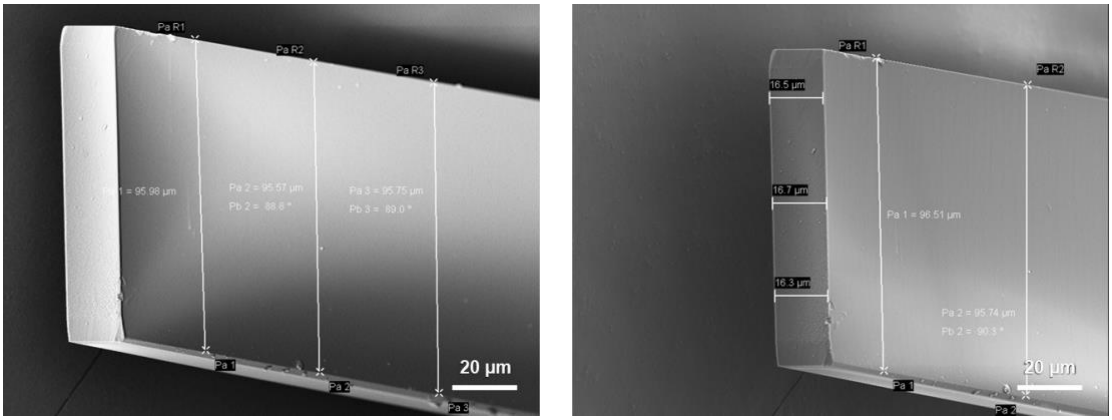

Fig. S11 SEM images of the rod-shaped crystal of **P2Mac** showing cross-sectional dimensions (W = 95.7 µm, H = 16.5 µm).

6.4.3 DC Conductivity Studies

Next, we investigated the DC proton conductivity of the crystals at room conditions (27 °C and 50% RH). The probes, in this case, were electrically charged with the help of a Keithley 2450 SMU, and the applied potential bias was varied from 0 to 2.5 V in steps of 0.05 V. The resistance was calculated from the slope of the current-voltage (*I*–*V*) plot and was 1.46 GΩ. Thereafter, the humidity inside the chamber was allowed to rise steadily to approximately 95% RH for 12 hours. Under the humid experimental conditions, the voltage sweep yielded a resistance of 1.37 MΩ. The DC conductivities at both humidity conditions were then calculated using Equation 2.

Table S4. Proton conductivity of previously reported single-component organic SSPC materials.

Sl. No.	*Sample*	σ_{AC} *(mS·cm^{-1})*	σ_{DC} *(mS·cm^{-1})*	*Condition*	E_a *(eV)*	*References*	*Year*
1	***p*-6PA-HPB**	25.0 (Pellet)	–	25 °C, 95% RH	–	4	2009
2	**1**	1.10 (Pellet)	–	30 °C, 95% RH	0.35	5	2016
3	**HOF-6a**	3.40×10^{-3} (Pellet)	–	27 °C, 97% RH	–	6	2016
4	**3˙**	–	9.20×10^{-1} (Pellet)	30 °C	0.15	7	2021
5	**Cage-1**	1.59×10^{-1} (Crystal pellet)	–	30 °C, 98% RH	0.16	8	2022
6	**1-H_2O**	12.0 (Crystal)	–	95 °C, 98% RH	0.54	9	2022
7	**ES-MA[6]**	–	7.50×10^{1} (Crystal)	27 °C	–	10	2023
8	**Yellow form**	1.20×10^{-1} (Pellet)	–	95 °C, 95% RH	0.098	11	2023
9	**Azo-DPA**	1.63×10^{-1} (Crystal pellet)	–	30 °C, 95% RH	0.23	12	2024
10	**P2Mac**	21.1 (Crystal)	9.70×10^{-1} (Crystal)	27 °C, 95% RH	–	*This work*	–
		1.79×10^{-1} (Pellet)	–	65 °C, 95% RH	0.39		

7. NMR Spectra

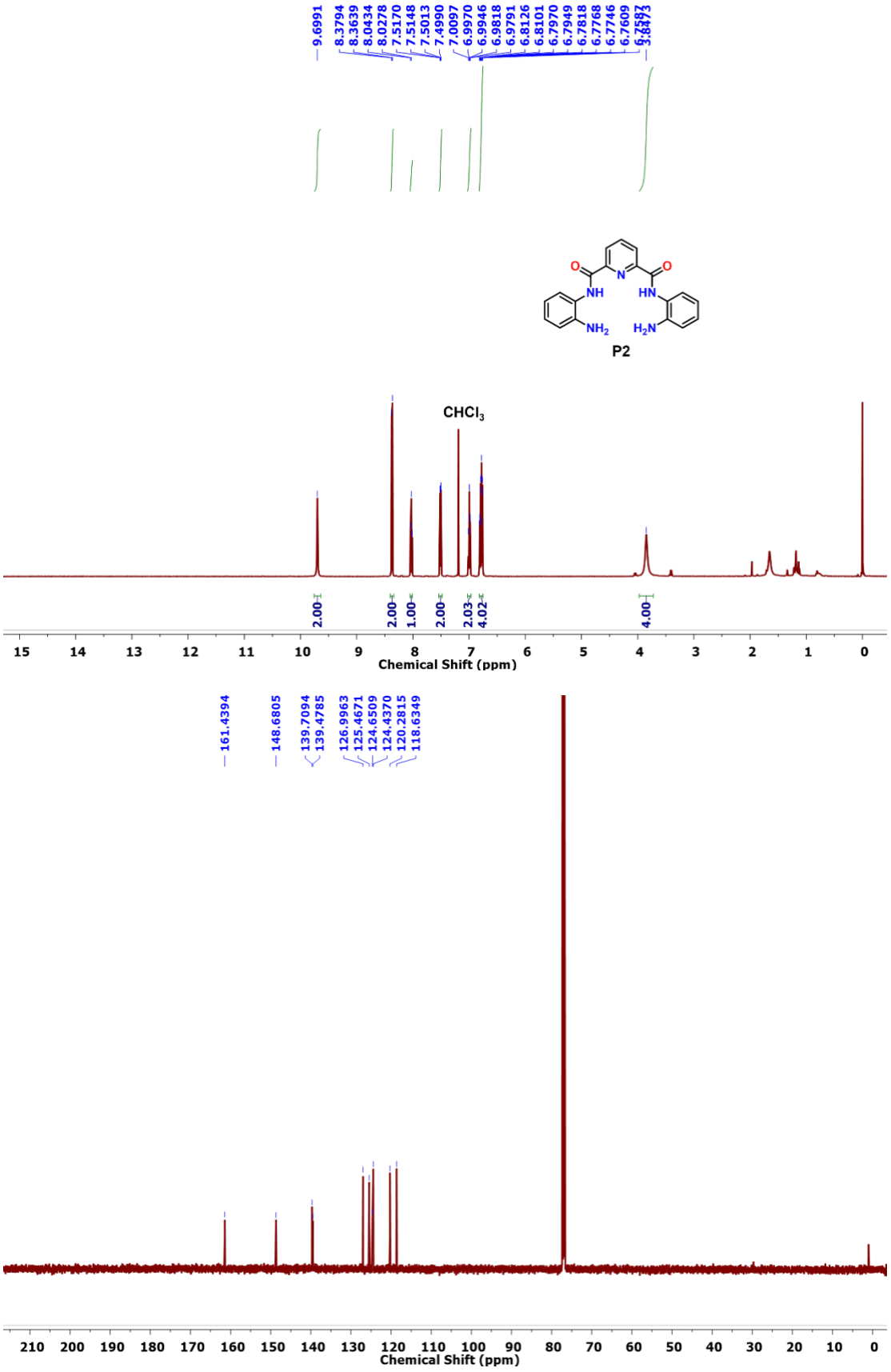

Fig. S12 ^{1}H (500 MHz) and ^{13}C NMR spectra (125 MHz) of precursor **P2** in $CDCl_3$, 25 °C.

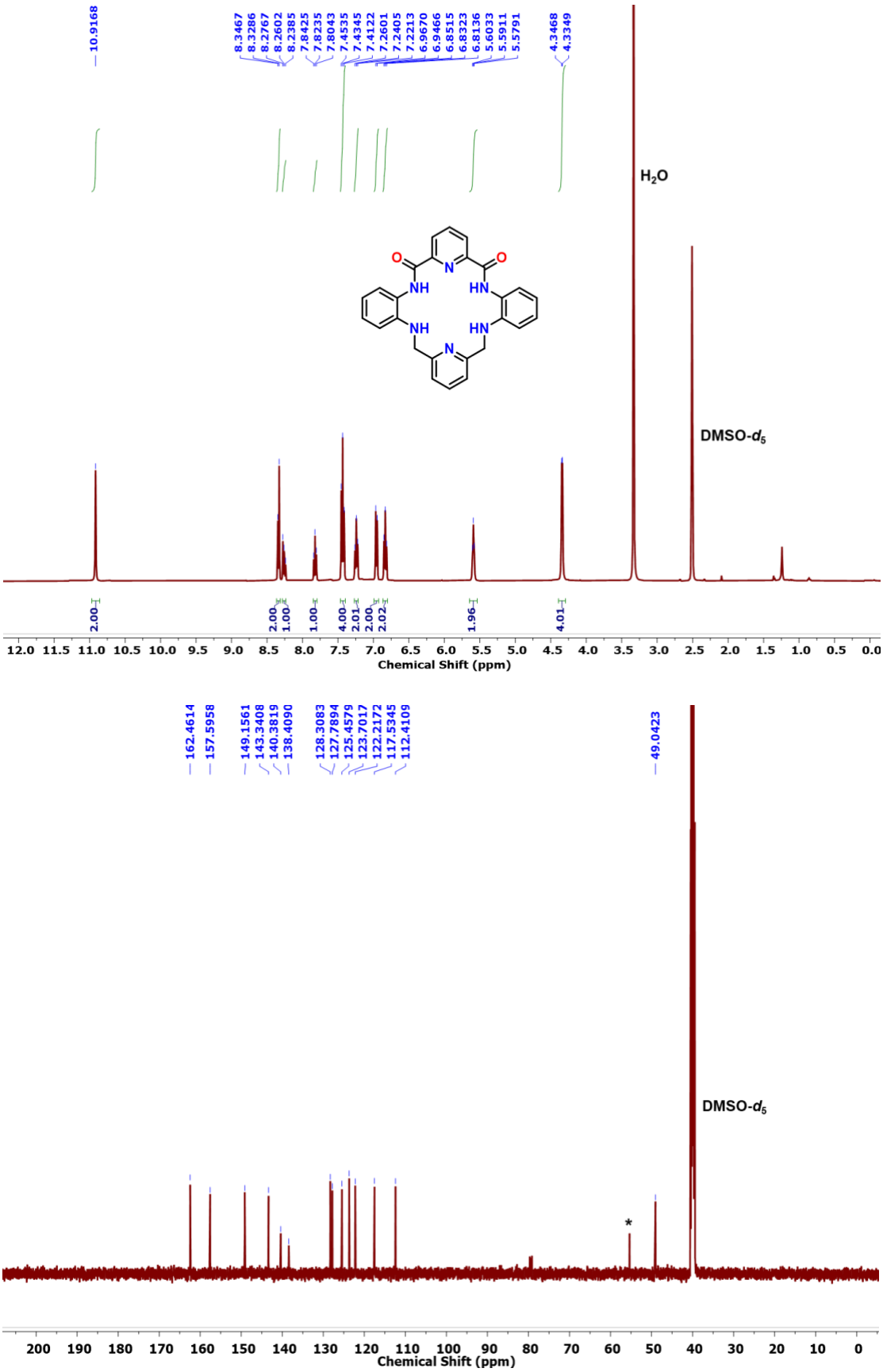

Fig. S13 ^{1}H (500 MHz) and ^{13}C NMR spectra (125 MHz) of **P2Mac** in DMSO-d_6, 25 °C.

8. References

1 O. V. Dolomanov, L. J. Bourhis, R. J. Gildea, J. A. K. Howard and H. Puschmann, *J. Appl. Crystallogr.*, 2009, **42**, 339–341.

2 Gaussian 09, Revision D.01, M. J. Frisch, G. W. Trucks, H. B. Schlegel, G. E. Scuseria, M. A. Robb, J. R. Cheeseman, G. Scalmani, V. Barone, B. Mennucci, G. A. Petersson, H. Nakatsuji, M. Caricato, X. Li, H. P. Hratchian, A. F. Izmaylov, J. Bloino, G. Zheng, J. L. Sonnenberg, M. Hada, M. Ehara, K. Toyota, R. Fukuda, J. Hasegawa, M. Ishida, T. Nakajima, Y. Honda, O. Kitao, H. Nakai, T. Vreven, J. A. Montgomery, Jr., J. E. Peralta, F. Ogliaro, M. Bearpark, J. J. Heyd, E. Brothers, K. N. Kudin, V. N. Staroverov, T. Keith, R. Kobayashi, J. Normand, K. Raghavachari, A. Rendell, J. C. Burant, S. S. Iyengar, J. Tomasi, M. Cossi, N. Rega, J. M. Millam, M. Klene, J. E. Knox, J. B. Cross, V. Bakken, C. Adamo, J. Jaramillo, R. Gomperts, R. E. Stratmann, O. Yazyev, A. J. Austin, R. Cammi, C. Pomelli, J. W. Ochterski, R. L. Martin, K. Morokuma, V. G. Zakrzewski, G. A. Voth, P. Salvador, J. J. Dannenberg, S. Dapprich, A. D. Daniels, O. Farkas, J. B. Foresman, J. V. Ortiz, J. Cioslowski, and D. J. Fox, Gaussian, Inc., Wallingford CT, 2013.

3 N. P. Pradhan, K. R. Namdev and A. Srivastava, *Org. Biomol. Chem.*, 2024, **22**, 74–79.

4 L. Jiménez-García, A. Kaltbeitzel, W. Pisula, J. S. Gutmann, M. Klapper and K. Müllen, *Angew. Chem. Int. Ed.*, 2009, **48**, 9951–9953.

5 M. Liu, L. Chen, S. Lewis, S. Y. Chong, M. A. Little, T. Hasell, I. M. Aldous, C. M. Brown, M. W. Smith, C. A. Morrison, L. J. Hardwick and A. I. Cooper, *Nat. Commun.*, 2016, **7**, 12750.

6 W. Yang, F. Yang, T.-L. Hu, S. C. King, H. Wang, H. Wu, W. Zhou, J.-R. Li, H. D. Arman and B. Chen, *Cryst. Growth Des.*, 2016, **16**, 5831–5835.

7 T. Murata, S. Matsui and G. Saito, *Mol. Cryst. Liq. Cryst.*, 2021, **730**, 23–34.

8 Z. Yang, N. Zhang, L. Lei, C. Yu, J. Ding, P. Li, J. Chen, M. Li, S. Ling, X. Zhuang and S. Zhang, *JACS Au*, 2022, **2**, 819–826.

9 M.-Y. Zhou, H.-Y. Wang, Z.-S. Wang, X.-W. Zhang, X. Feng, L.-Y. Gao, Z.-C. Lian, R.-B. Lin and D.-D. Zhou, *Chem. Commun.*, 2022, **58**, 771–774.

10 S. Louie, Y. Zhong, S. T. Bao, C. Schaack, A. Montoya, Z. Jin, N. M. Orchanian, Y. Liu, W. Lei, K. Harrison, J. Hone, A. Angerhofer, A. M. Evans and C. P. Nuckolls, *J. Am. Chem. Soc.*, 2023, **145**, 4940–4945.

11 H. Aggarwal, P. A. Gaikwad, A. Dahat, S. Narayan Ghosh, P. Mehra, A. Paul, S. Talukder and A. Srivastava, *Chem. – Eur. J.*, 2023, **29**, e202300019.

12 M. S. Hossain, M. Ghosh, A. Mondal, A. P, M. Saha, C. M. Reddy, S. Kurungot and S. Bandyopadhyay, *J. Mater. Chem. A*, 2024, **12**, 5866–5874.